ICARUS 83, 282–307 (1990)

Planetary Waves in Jupiter's Equatorial Atmosphere

MICHAEL ALLISON

NASA/Goddard Institute for Space Studies, 2880 Broadway, New York, New York 10025

Received June 6, 1988; revised June 20, 1989

Voyager infrared, radio occultation, and imaging measurements provide a variety of observational evidence and constraints for planetary-scale waves latitudinally trapped within Jupiter's equatorial jet. The visually prominent plumes, encircling the planet at 8 deg north latitude, show a longitudinal organization of wavenumber $n \approx 11$–13. An apparently solitary plume also appears at about 8 deg south along with other smaller periodic cloud features. Deviations in cloud-tracked drift speeds (including differences in mean values to the north and south of the equator) in excess of 25 m sec^{-1} may be crudely indicative of the magnitude of the associated wave phase speeds. Radio occultation retrievals of the temperature profiles at two equatorial longitudes show harmonic variation consistent with the stratospheric propagation of two components with vertical wavelengths of approximately 3 and 0.5 scale heights. These observations may be consistently interpreted in terms of specific classes of equatorially trapped wave modes. The gravest equatorial Rossby mode with an "equivalent depth" of $h \approx 2$–4 km (with a stratospheric wavelength of 3–4 scale heights) represents the most consistent interpretation of the plumes. The inferred vertical eigenmode could be ducted by a deep, statically stable layer, possibly imposed by a roughly solar abundant water cloud, depending upon the actual details of the moist convection. An estimate of the relative growth rates for the near-neutral forcing of Rossby modes of the inferred equivalent depth implies a maximum for zonal wavenumber 11. The solitary plume feature to the south of the equator may be interpreted as a wavenumber 1 Rossby mode with the same vertical scale, possibly forced by the interaction between the equatorial jet and the Great Red Spot. Smaller visual features may correspond to inertia–gravity modes with vertical wavelengths comparable to the small harmonic of the occultation profiles. Galileo orbiter and probe observations will provide an essential test of the wave analysis and substantially enhance its diagnostic utility.

1. INTRODUCTION

Except for the Great Red Spot, Jupiter's equatorial plumes are the most prominent longitudinal features on the planet. These are clearly evident even in several historical drawings of the planet (cf. Focas and Banos 1964, Peek 1981). They appear to be confined between 2 and 9 deg north latitude, are more or less evenly spaced in longitude, and at the time of the Voyager encounters numbered between 11 and 13. The features are embedded within Jupiter's wide equatorial jet, where the eastward flow velocity is about 100–130 m sec^{-1}. The coincidence of this latitudinal region with the currently planned entry site for the Galileo atmospheric probe makes it especially pertinent for further study in advance of the *in situ* observations of its vertical structure.

Several investigators have suggested that the plumes may be interpreted as the effect of organized wave propagation (cf. Smith *et al.* 1979, Mitchell *et al.* 1979, Hunt *et al.* 1981) but without attempting to analyze their dispersion properties and associated vertical structure. Although the wavenumber 11 plume pattern appears to be absent to the south of the equator, Voyager imaging observations show a single large but

0019-1035/90 $3.00

morphologically similar feature there at about 8 deg latitude. According to Maxworthy (1985) the south equatorial plume drifts to the west with respect to the mean cloud-tracked wind at a speed of several tens of meters per second and may be interpreted as a Rossby solitary wave. Other discrete but much smaller cloud features are also apparent at about the same latitude. An independent and especially tantalizing suggestion of equatorial wave activity is evident in the vertical temperature profiles retrieved from Voyager radio occultations at two equatorial locations (Lindal *et al.* 1981), showing a two-component periodic oscillation corresponding to wave lengths of about 3 and 0.5 scale heights.

Two features of the theory of planetary-scale waves, as developed for terrestrial meteorology, appear to be relevant to the Jupiter observations. Lindzen (1967) and others have shown that midlatitude disturbances of sufficiently high frequency and large spatial scale are vertically trapped. Within regions sufficiently close to the equator, however, disturbances of any frequency can, in the absence of strong wind shear, propagate vertically away from their level of excitation. In addition, the theory demonstrates that equatorial oscillations of sufficiently large (planetary) scale are meridionally trapped, even in the absence of horizontal shear, as a result of the rapid variation there in the latitudinal gradient of the local normal projection of the planetary rotation frequency (the so-called beta effect). The first feature is consistent with the apparent oscillation in the two equatorial profiles determined by Voyager radio occultations as compared with a third profile obtained by the same method at higher latitudes (57–73 deg) showing relatively little vertical variation about the mean stratospheric lapse rate (Lindal *et al.* 1981). The second (meridional trapping) feature of the equatorial wave theory is consistent with the confinement of the plumes to within about 8 deg latitude of the equator, well within the half-width of Jupiter's equatorial jet.

The diagnostic analysis of planetary waves in the Earth's tropics has proceeded by the comparison of the linear dispersion relations to the power spectrum of their observed oscillation frequencies and their measured phase drift in time-composite satellite photographs (cf. Wallace and Chang 1969, Chang 1970, Holton 1970, Lindzen 1974b). A comprehensive review of both the theory and observations of tropical waves in the Earth's atmosphere and ocean is given by Beer (1978). Although the determination of the oscillation frequency of planetary waves in Jupiter's atmosphere is much more problematic, measured deviations in cloud-tracked drift speeds (including their differences to the north and south of the equator) may serve as a rough indication of allowable horizontal phase velocities. The diagnostic assessment of the equatorial eigenmodes is also constrained by the observed latitudal position of the plumes. The application of these constraints, including the vertical structure of the radio occultation profiles, permits the preliminary identification of certain distinguishing classes of linear wave modes consistent with all the observations.

2. OBSERVATIONS

A number of images showing the prominent cloud features within Jupiter's equatorial region have been published by various Voyager investigators (cf. Smith *et al.* 1979, Ingersoll *et al.* 1979). Figure 1 shows a mosaic assembled from near-encounter orange-filtered Voyager 1 images of the equatorial region, showing both the north equatorial plumes and the single prominent south equatorial feature. Their longitudinal wavenumbers may be identified by visual inspection as $n = 11$–13 and $n = 1$, respectively. Hunt *et al.* (1979) have performed a correlative study of Voyager images and IRIS temperatures for the north equatorial plumes. They report that the thermal struc-

FIG. 1. Voyager imaging mosaic of Jupiter's equatorial region. The orange-filtered images were recorded during the near-encounter north–south mapping sequence by the Voyager 1 narrow-angle camera on March 3, 1979. The mosaic has been assembled by the author without correction for the variation of viewing angle and distance with time so that some distortion between individual frames is evident. The equatorial strip covers approximately ±23 deg of planetographic latitude and 160 deg of longitude, running from approximately 200 deg (System III) on the left to 40 deg on the right. Six of the equatorial plume centers are visible to the north of the equator. The southern equatorial plume feature is also evident within the third column of frames from the left and, at about the same latitude, the small-scale chevron structure. The Great Red Spot appears prominently within the second column from the right.

ture above the cloud deck also shows a periodic variation consistent with tropospheric wave activity on the same longitudinal scale as the northern plumes and which appears to be vertically coherent over infrared sounding levels between 150 and 700 mbars. (Since the vertical resolution of the IRIS retrievals does not permit the detection of an oscillation with a vertical wavelength smaller than about two scale heights, this may be taken as a rough lower limit for the observed structure.)

Periodic structure on much smaller horizontal scales is also apparent in the Voyager images of the equatorial region. Small-scale cloud striations with typical longitudinal separations of 300 km (roughly 100 times smaller than the spacing of the north equatorial plumes) have been catalogued by Flasar and Gierasch (1986) and interpreted as mesoscale gravity waves but are by any reckoning subplanetary scale phenomena. In addition, the Voyager images show small-scale periodic structure at latitude 8 deg south with a longitudinal regularity consistent with zonal wavenumbers of $n \sim 50$–100. (This is the chevron pattern apparent in Plate 10a of Ingersoll *et al.* 1979 and is also visible in Fig. 1 of this paper.)

Maxworthy's (1985) cloud-tracked wind measurements of Voyager images of the large south equatorial plume indicate a westward wave phase velocity for this feature of about 70 m sec^{-1} with respect to the mean flow at the same latitude. Although there are apparently no such dramatic differences in the measured cloud-tracked

drift velocity at the latitude of the north equatorial plumes, the root-mean-square deviation of measured velocities there, as determined by Ingersoll *et al.* (1981) and Limaye *et al.* (1982), is as large as 20 m sec^{-1}. There is also a measured north–south asymmetry in the cloud-tracked drift speed near the maxima of the otherwise symmetric equatorial jet profile, with velocities at 8 deg north some 25–30 m sec^{-1} smaller than those at 8 deg south (cf. Ingersoll *et al.* 1981, Limaye 1986). If the north equatorial plumes and the associated cloud structure are the only features which can be tracked at their latitude (cf. Fig. 1), then the observed difference may be the effect of westward phase velocities embedded in a symmetric flow profile. If the measured wind vectors associated with the apparent variety of cloud features just to the south of the equator are some admixture of the effects of mass motion and westward phase drift, then the north equatorial plumes might themselves have a westward phase velocity somewhat in excess of 30 m sec^{-1}.

Although the latitudinal asymmetry in the measured wind profile may be a real indication of differential mass motion at the same altitude, the relative drift of the southern plume is difficult to discount except perhaps as a marker of slower motion at a higher elevation. The combined effect of differential cloud elevation and vertical wind shear (cf. Maghales *et al.* 1987, Limaye 1987) is only crudely constrained by presently available measurements. The thermal wind analysis of Voyager IRIS data by Gierasch *et al.* (1986) indicates that the vertical shear above the cloud deck at this latitude amounts to less than 40 m sec^{-1} per scale height while Coffeen's (1974) analysis of Pioneer polarimetry data implies that the range of variation of the upper cloud levels across Jupiter's equatorial zone is much less than a scale height. Although these estimates would appear to suggest that differential elevation and shear are insufficient to account for all the apparent relative drift in this region, the limited spatial resolution of the thermal data as well as model-dependent uncertainties in the cloud-height analysis will not admit a firm conclusion. The considered observational allowances on the phase velocity are best regarded as crude characterizations of the plausible limits. Although phase velocities exceeding the maximum observed flow speed may be excluded, for example, phase drifts up to about half the jet speed probably are not. Phase velocities much less than mean flow differences across the jet (~30 m sec^{-1}) may be susceptible to absorption by latitudinal shear.

Perhaps the single most persuasive evidence for wave activity in Jupiter's equatorial atmosphere is provided by the Voyager radio occultation profiles reported by Lindal *et al.* (1981). Figure 2 displays the results in comparison with a Voyager IRIS profile (with a vertical resolution of about 2 scale heights) and a constant static stability profile (in log–pressure coordinates, as pre-

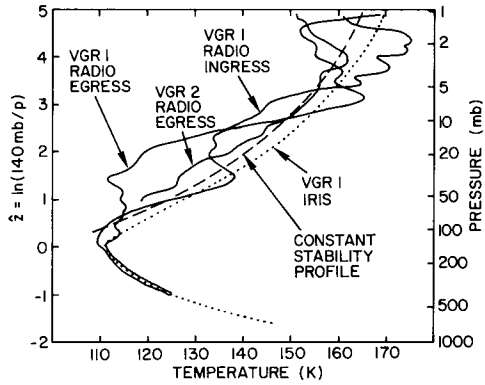

FIG. 2. Temperature profiles for Jupiter's upper atmosphere. The solid curves are from radio occultation retrievals (after Lindal *et al.* 1981). The Voyager 1 ingress measurement was taken at 11–12 deg south latitude and 62–68 deg longitude; the Voyager 1 egress at 0–1 deg north latitude and 307–313 deg longitude; the Voyager 2 egress at 57–73 deg south latitude and 124–144 deg longitude. The dotted Voyager 1 IRIS profile was retrieved from the average of 13 interferogram measurements taken during the time of the occultation ingress (supplied by private communication from Barney Conrath). The dashed curve is for a constant static stability of Γ/g = 10 km, chosen to represent the mean stratospheric profile.

scribed in Section 3) corresponding to an ambient temperature

$$T^a = -78°K \cdot \exp[-(R/c_p)\hat{z}] + 180°K \quad \text{for } \hat{z} > 1, \quad (1)$$

and appears to be a good mean representation of the data. (Here $R/c_p \approx 0.34$ denotes the ratio of the gas constant to the specific heat at constant pressure.) The Voyager 1 ingress and egress measurements were obtained for near-equatorial latitudes while the Voyager 2 egress measurement was obtained for high southern latitudes (between 57 and 73 deg). The Voyager 2 high latitude profile nearly coincides with the assumed constant stability profile over three scale heights (between 50 and 2 mbars). The vertical variations of both Voyager 1 equatorial profiles indicate a 10°K oscillation over a wavelength of 3 scale heights. There is also a suggestion of a second harmonic of 2°K amplitude and a vertical wavelength of about half a scale height. Figure 3 displays a comparison of the equatorial profiles with simple model fits consisting of the two harmonics superimposed on the constant stability profile. Since the occultation retrievals are essentially "snapshots" of the thermal structure, they contain no direct information about wave frequency. They also contain no specific information regarding the horizontal wavenumber of the oscillation, except that the longitudinal resolution reported by Lindal *et al.* (1981) will not admit to the detection of features much smaller than about zonal planetary wavenumber 100. It is possible that the observed structure is due to the radiative–convective equilibrium of some peculiar vertical distribution of absorbing constituents. Appleby and Hogan (1984) have investigated this possibility with radiative–convective equilibrium models but conclude that a somewhat *ad hoc* alternation of aerosol heating and cooling with altitude is required to match the radio occultation profiles and that the implied energy balance is not obviously compelling. The remarkable resemblance of the simple model profiles in Fig. 3 to the observations at two different equatorial locations and for separate phases (by coincidence nearly 180° apart for the largest harmonic) would appear to be most plausibly interpreted as a wave-dynamical phenomenon.

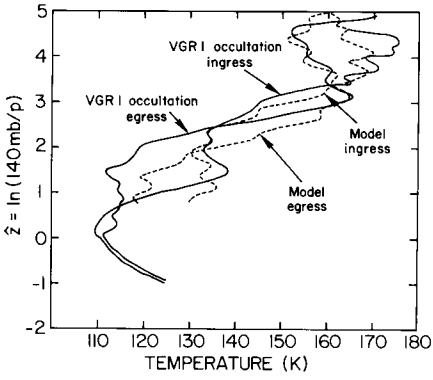

FIG. 3. Simple model fits to the Voyager 1 radio occultation profiles. The solid curves are based on equatorial observations reported by Lindal *et al.* (1981) as also shown in Fig. 2. The dashed curves are simple model fits obtained from the sum of the constant stability profile shown in Fig. 2 and two harmonic components with amplitude, wavelength, and phase chosen to match the observations. The large harmonic is fitted with a wavelength of 3 scale heights and an amplitude of 10°K, the small harmonic with a wavelength of 0.5 scale heights and an amplitude of 2°K.

3. DIAGNOSTIC WAVE THEORY

The diagnostic analysis of the various periodic features summarized above may be approached in terms of the linear wave dynamics for an equatorial beta plane. The effects of planetary curvature on large-scale motions are accounted for by specifying the latitudinal gradient of the Coriolis parameter as $\beta = df/dy = 2\Omega/a$, where Ω and a are respectively the planetary rotation frequency and radius. Although the theory is mostly standard (cf. Lindzen 1967 or Pedlosky 1987), for the sake of clarity and completeness in its present application the essential relations will be set down here. In log–pressure coordinates the linearized equations for hydrostatic perturbations on an equatorial beta plane with

constant mean flow advection, horizontal momentum dissipation, and diabatic heating read

$$\partial u/\partial t + U \cdot \partial u/\partial x - \beta y v + \partial \phi/\partial x = \mathfrak{D}\mathbf{x} \tag{2}$$

$$\partial v/\partial t + U \cdot \partial v/\partial x + \beta y u + \partial \phi/\partial y = \mathfrak{D}\mathbf{y} \tag{3}$$

$$\partial \phi/\partial \hat{z} - RT = 0 \tag{4}$$

$$\partial u/\partial x + \partial v/\partial y + (\partial/\partial \hat{z} - 1)\hat{w} = 0 \tag{5}$$

$$\partial T/\partial t + U \cdot \partial T/\partial x + \Gamma \hat{w}/R = \mathbf{Q}. \tag{6}$$

The symbols and constants to be employed in the analysis are defined as follows:

$t, x, y, \hat{z} \equiv \ln(p_0/p)$	time, eastward, northward, and upward coordinates
ϕ, T	(wave) geopotential height, temperature
$u, v, \hat{w} \equiv d\hat{z}/dt$	eastward, northward, upward (wave) velocities
U	eastward mean flow velocity (of equatorial jet)
n	zonal (planetary) wavenumber
$\mu, \mathscr{L}_{\hat{z}}$	vertical (log $-$ p) wavenumber, vertical wavelength
c	horizontal phase velocity relative to mean flow
$\sigma = (n/a)c$	(Doppler-shifted) frequency relative to mean flow
h	equivalent depth of vertical wave structure
$\Gamma = R(\partial T^a/\partial \hat{z} + RT^a/c_p)$	static stability parameter
T^a	ambient static temperature
$\mathfrak{D}\mathbf{x}, \mathfrak{D}\mathbf{y}$	horizontal (x and y) momentum dissipation (or driving)
$\mathbf{Q}$	diabatic heating (or damping) rate
$\Omega = 1.76 \times 10^{-4}$ sec^{-1}	planetary rotation frequency (Jovian System III)
$a = 7.14 \times 10^7$ m	(equatorial) planetary radius
$\beta = 4.93 \times 10^{-12}$ m^{-1} sec^{-1}	(equatorial) beta parameter
g = 23 m sec^{-2}	gravitational acceleration (for equatorial zone)
$R = 3.7 \times 10^3$ m^2 sec^{-2} °K^{-1}	gas constant (for a Jupiter H_2–He mixture)
$c_p = 1.1 \times 10^4$ m^2 sec^{-2} °K^{-1}	specific heat at constant pressure (Jupiter mixture)
$p_0 = 140$ mbars	reference pressure level for which $\hat{z} \equiv 0$.

All dependent field variables are taken to represent wave perturbations. Phase velocities and frequencies will be referenced with respect to the mean flow of the equatorial jet. Westward (or easterly) phase velocities will be taken to correspond to negative values for both c and σ, so that the zonal planetary wavenumber n may always be taken as positive. The diagnostic application of Eqs. (2)–(6) to the separate observational constraints on the vertical and horizontal structure of planetary wave phenomena is facilitated by the initial neglect of forcing, dissipation, and shear. Some of the effects of these will be considered in Section 5 but without a substantial alteration in the diagnostic assessment of the wave dispersion properties. The *a priori* neglect of horizontal shear is required in order to maintain a tractable diagnostic analysis but may be partly justified by the observation that the plumes are meridionally confined without a region of the equatorial jet where the integrated horizontal shear amounts to less than 45 m sec^{-1}.

With $\mathfrak{D}\mathbf{x} = \mathfrak{D}\mathbf{y} = \mathbf{Q} = 0$, and assuming solutions harmonic in time and longitude of the form $e^{i(n/a)(x-ct)}$, where n is the zonal planetary wavenumber and c the horizontal phase velocity relative to the mean flow speed U, Eqs. (2)–(6) may be reduced to a single equation in v:

$$\frac{\partial^2 v}{\partial y^2} - \left(\frac{n}{a}\right)^2 v - \frac{\beta}{c} v + \left(\frac{\partial}{\partial \hat{z}} - 1\right) \frac{(\beta y)^2 - (cn/a)^2}{\Gamma} \frac{\partial v}{\partial \hat{z}} = 0. \quad (7)$$

Now the horizontal and vertical structure may be separated by setting

$$v(y, \hat{z}) = \sum_j \psi_{j,n}(y) \cdot G_{j,n}(\hat{z}). \quad (8)$$

The horizontal structure is then determined (for each choice of j) by

$$\frac{d^2\psi}{dy^2} + \left[\frac{(cn/a)^2 - (\beta y)^2}{gh} - \frac{\beta}{c} - (n/a)^2\right] \psi = 0, \quad (9)$$

where gh has been introduced as the separation constant. (h is called the "equivalent depth" and corresponds to the thickness of an incompressible fluid with the same horizontal structure properties. Although the introduction of the gravitational acceleration parameter is not essential here, the equivalent depth nomenclature serves to emphasize the relationship between the present analysis and the standard "shallow water" theory as well as many of the referenced studies of terrestrial meteorology.)

The equation for G is simplified by the transformation

$$\chi = e^{-\hat{z}/2} \frac{g}{\Gamma} \frac{dG}{d\hat{z}} \quad (10a)$$

or equivalently

$$G = -h \cdot e^{+\hat{z}/2} \left(\frac{d\chi}{d\hat{z}} - \frac{1}{2}\chi\right) \quad (10b)$$

so that the vertical structure equation may be written as

$$\frac{d^2\chi}{d\hat{z}^2} + \left(\frac{\Gamma}{gh} - \frac{1}{4}\right)\chi = 0. \quad (11)$$

Vertical propagation will therefore occur for $0 < h < 4\Gamma/g$, with a vertical wavelength (for a fixed static stability) of $\mu = (\Gamma/gh - \frac{1}{4})^{1/2}$. Otherwise the wave is vertically trapped. With an ambient static temperature given by (1), the same as the dashed model curve plotted in Fig. 2, $\Gamma/g \approx 10$ km. Then with a vertical wavelength of $2\pi/\mu \approx 3$ scale heights in the lower stratosphere, as evidenced by the radio occultation retrievals, an equivalent depth of $h \approx 2.2$ km is indicated, while the smaller harmonic with $2\pi/\mu \approx 0.5$ scale heights corresponds to $h \approx 0.06$ km. At upper tropospheric levels around 300 mbars the static stability may be estimated from the IRIS and radio occultation retrievals as $\Gamma/g \approx 2$ km. Then the vertical wavelength for $h \approx 2.2$ km at this level amounts to several scale heights and, even for $h \approx 0.06$ km, is greater than one log-pressure interval, consistent with the absence of oscillatory structure in the retrieved tropospheric profiles. At still deeper tropospheric levels, the static stability may be expected to be even smaller as the ambient lapse rate approaches the adiabat so that $\Gamma/g < h/4$. There the wave fields will be approximately constant with altitude above their level of excitation or trapping and presumably exponentially damped below.

The horizontal structure equation (9), has the same form as the Schroedinger equation for the harmonic oscillator and the (normalized) solutions

$$\psi_j = [(2^j j! \pi^{1/2})^{-1/2}] \cdot e^{-\eta^2/2} H_j(\eta), \quad \text{with } \eta \equiv (\beta/\sqrt{gh})^{1/2} y, \quad (12)$$

where the $H_j(\eta)$ are the Hermite polynomials, with $j = 0, 1, 2, \ldots$ ($H_0 = 1$, $H_1 = 2\eta$, $H_2 = 4\eta^2 - 2$, etc.) The associated eigencondition for the decay of solutions as $\eta \to \pm\infty$ is

$$\left(\frac{\sqrt{gh}}{\beta}\right)\left[\frac{(cn/a)^2}{gh} - \frac{\beta}{c} - (n/a)^2\right] = 2j + 1. \quad (13)$$

The meridional solutions to the horizontal structure equation (9) will evidently decay with increasing y in regions where the

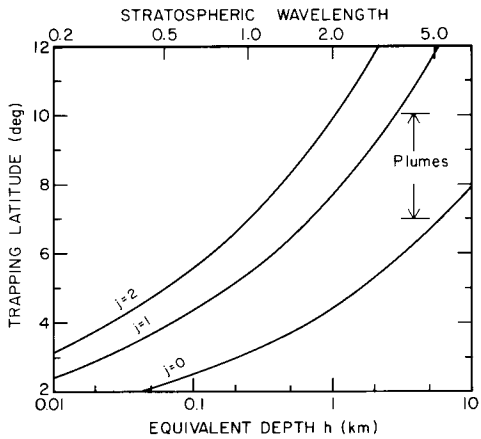

FIG. 4. The approximate meridional trapping scale (in degrees latitude) vs the equivalent depth (in km) for the $j = 0$, 1, and 2 modes on a Jovian equatorial beta plane.

term in brackets is negative which, by comparison with the eigencondition (13), occurs for all y in excess of the value given by

$$y_d^2 = (2j + 1)\sqrt{gh}/\beta. \qquad (14)$$

Figure 4 displays the variation of this meridional trapping distance, converted to degrees latitude, as a function of the equivalent depth for $j = 0$, 1, and 2. This shows at once that for the $j = 1$ and 2, $h \sim 2$ km modes, the meridional decay scale is approximately 9 deg, in good agreement with the observed latitude of the plume centers. For $h \sim 0.06$ km and the same choices for j it is only about half their equatorial offset distance. (The full meridional shape of the geopotential and vertical velocity eigenfunctions will be illustrated below.)

The eigencondition (13), rearranged in the form of the dispersion relation prescribing the wavenumber dependence of the horizontal phase velocity for all the equatorial wave modes, reads

$$\left(\frac{c}{\sqrt{gh}}\right)^3 - \left[1 + \frac{(2j + 1)\beta a^2}{n^2\sqrt{gh}}\right]\left(\frac{c}{\sqrt{gh}}\right) - \frac{\beta a^2}{n^2\sqrt{gh}} = 0. \qquad (15)$$

This fortuitously includes, for the choice of $j = -1$, the Kelvin mode not covered by (7) for which the meridional velocity everywhere vanishes. (The vertical structure equation is the same.) The general dispersion relation includes gravity waves, for which inertial accelerations are balanced by buoyant stability to vertical displacement, as well as Rossby waves, for which the inertial balance depends instead upon the planetary vorticity gradient β over the ambient field of latitudinal excursions. For midlatitude motion systems gravity waves are typically restricted to small-scale oscillations with frequencies much greater than the local Coriolis parameter $f \equiv 2\Omega \sin \lambda$, while the large-scale Rossby waves (of horizontal wavelength $L \sim a/n$) have much lower frequencies, comparable to $f \cdot (L/a)$. Within the equatorial trapping region, where the Coriolis parameter is very small, the two types of waves are more essentially convolved. It is useful, however, to consider in detail the distinctive dispersion properties of individual modes corresponding to the different choices of the meridional structure index j.

j = −1. For this choice (15) has only the one physical solution (consistent with bounded behavior of the wave fields) corresponding to the eastward propagating Kelvin wave with a phase speed

$$c_{\text{Kelvin}} = \sqrt{gh}. \qquad (16)$$

This mode is exactly nondispersive (with a phase speed independent of the zonal wavenumber) and resembles a shallow water gravity wave of depth h. Its meridional structure is that of a Gaussian, maximum on the equator, with an e-folding scale of $[2\sqrt{gh}/\beta]^{1/2}$ and a half-width at half-maximum amplitude very nearly the same as the decay scale for the $j = 0$ mode shown in Fig. 4.

j = 0. For this choice Eq. (15) yields one nonphysical root corresponding to a westward Kelvin mode which is excluded by the divergence of the associated wave field with latitude. The physical solutions, called

the mixed Rossby-gravity or Yanai modes, are given by

$$c_{\text{Yanai}} = (\sqrt{gh}/2)[1 \pm (1 + 4\beta a^2/n^2\sqrt{gh})^{1/2}]. \quad (17)$$

With the positive choice for the square root the phase speed is eastward and greater than the Kelvin speed which it asymptotically approaches in the limit of high zonal wavenumbers. With the negative square root the phase speed is westward and asymptotic to the short wave (large n) limit for Rossby waves discussed below.

$j \geq 1$. For this choice of j Eq. (15) yields two inertia–gravity modes, one propagating to the east, the other to the west, and one westward Rossby mode. These modes may be separately considered as follows. (The validity of the separation may be verified afterward from the indicated values for the phase speeds.)

(a) For the inertia–gravity case the phase speeds are given approximately by the balance between the first two terms of (15) so that

$$c_{\text{I-G}} \cong \pm\sqrt{gh}[1 + (2j + 1)\beta a^2/n^2\sqrt{gh}]^{1/2}. \quad (18)$$

The magnitude of the phase speed in this case is always greater than the Kelvin speed which it asymptotically approaches in the limit of large n, the same as the high zonal wavenumber limit of midlatitude inertia–gravity waves.

(b) For the equatorial Rossby mode the phase speeds are given by the balance between the last two terms of Eq. (15) so that

$$c_{\text{Rossby}} \cong \frac{-\beta a^2/n^2}{1 + (2j + 1)\beta a^2/n^2\sqrt{gh}}. \quad (19)$$

These are exclusively westward phase speeds with much lower frequencies (for the same equivalent depth) than the Kelvin and inertia–gravity modes. In the short wave limit $c_{\text{Rossby}}(n \to \infty) = -\beta a^2/n^2$, independent of the equivalent depth. In the long wave limit $c_{\text{Rossby}}(n \to 0) = -\sqrt{gh}/(2j + 1)$, so that for the gravest ($j = 1$) mode large-scale Rossby waves have a westward phase speed independent of βa^2 and nearly one-third that of the eastward Kelvin waves of the same equivalent depth.

The dispersion relations for the horizontal phase speed as a function of the zonal planetary wavenumber n are displayed in Fig. 5 over a range of several decades in the equivalent depth and for $j = -1, 0, 1$, and 2. (The ordinate gives the absolute value of the horizontal phase velocity.) This graphical "atlas" of equivalent depths over n and $|c|$ is a useful template for the diagnostic assessment of the modal character of the observed periodic variations in Jupiter's atmosphere. Smith *et al.* (1979a) have remarked that since atmospheric wave velocities are strong functions of wavelength, the agreement between measured velocities for features of different scale suggests that mass motion rather than wave propagation is observed in the Voyager imaging. Figure 5 shows, however, that in addition to the exactly nondispersive Kelvin solution, the Rossby modes are nearly nondispersive (with a phase speed only weakly dependent on the wavenumber) for equivalent depths less than about 3 km and $n < 15$, as are the eastward Yanai and inertia–gravity modes for equivalent depths greater than about 0.03 km and $n > 50$.

The horizontal phase speeds for the Kelvin ($j = -1$) and eastward Yanai ($j = 0$) modes with $h \sim 2$ km and $n < 15$ are all in excess of any cloud-tracked speeds ever observed on Jupiter. The phase speed for the highly dispersive westward Yanai mode, for $h \approx 2$ km and $n \approx 12$, amounts to about 100 m sec^{-1} and may also be ruled out as a likely candidate for any wave field associated with the north equatorial plume pattern. (Consistency with the cloud-tracked drift speeds would otherwise require a north equatorial velocity in excess of 200 m sec^{-1}.) Similarly, for the case of $j = 1$ and 2, the inertia–gravity modes may also be ruled out for a comparable equivalent depth and zonal wavenumber, again on account of apparently unrealistic phase

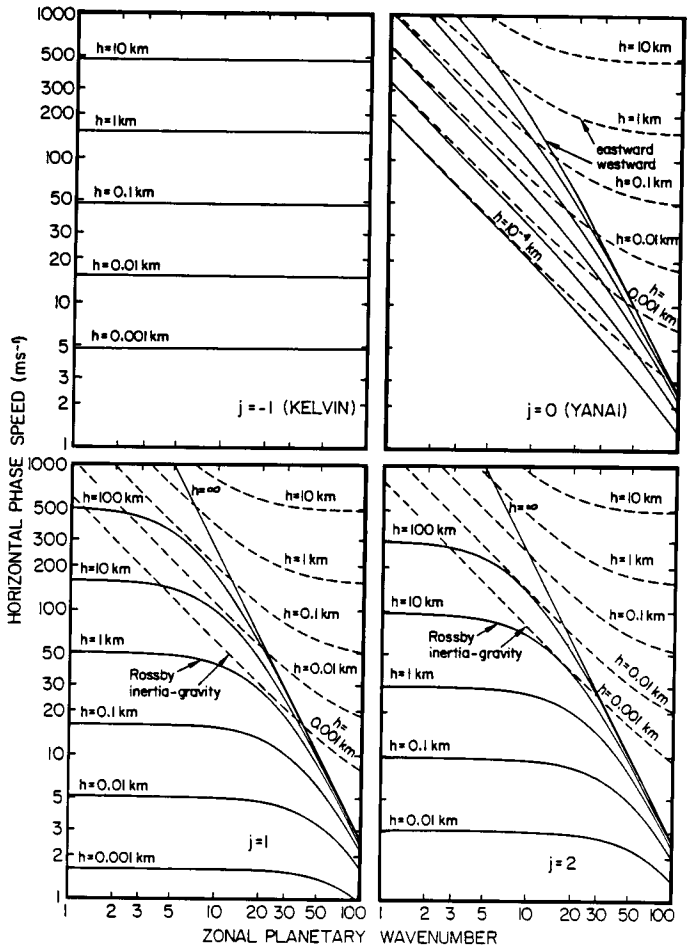

FIG. 5. Atlas of Jovian equivalent depths in the (n, c) plane: planetary wavenumber vs horizontal phase speed (with respect to the mean flow) on an equatorial beta plane for neutral linear modes.

speeds. The associated $j = 1$ and 2 Rossby modes, however, have (westward) phase velocities comparable to the observational constraints. For $h \approx 2$ km and $n < 20$, these are between 25 and 75 m sec^{-1}. For $j = 1$, $h = 2.2$ km, and $n = 13$, for example, the Rossby speed is 50 m sec^{-1}. The $j = 2$ Rossby mode has a smaller phase velocity than the $j = 1$ mode for the same choices of equivalent depth and wavenumber and might be vulnerable to critical layer absorption either by horizontal or vertical shear in the equatorial jet.

To the extent that the south equatorial plume feature can be identified with a linear $n = 1$ wave mode, similar considerations again lead to the Rossby wave as the preferred choice. With $j = 1$, $h = 2.2$ km, and $n = 1$, the Rossby speed is 75 m sec^{-1}, in good agreement with Maxworthy's (1985) estimate of its phase velocity. For the smaller vertical structure harmonic inferred from the radio occultation profiles, with $h \approx 0.06$ km, the phase speed relations displayed in Fig. 5 suggest that for sufficiently large n the eastward Yanai and inertia–gravity modes are both possible identifications. One or more of these are plausible identifications for the south equatorial chevron features (cf. Fig. 1) with $n > 50$.

Thermal and visual features may be expected to trace the variation of some combination of the geopotential, temperature, and vertical motion field of the waves more than the meridional velocity as employed in the horizontal structure equation above. The full solutions for these are somewhat elaborate but are summarized in Appendix A. Their latitude of maximum amplitude depends not only on the equivalent depth but also, for $j > 0$, weakly on the zonal wavenumber. As a representative illustration, Fig. 6 displays the relative meridional structure of the geopotential height field associated with a $j = 1$, $n = 12$, $h = 3$ km Rossby mode and the $j = 0$, $n = 12$, $h = 0.038$ km westward Yanai mode, along with the $j = 1$ and 2 eastward inertia–gravity modes for $n = 100$ and $h = 0.038$. The eigenfunction amplitudes have been arbitrarily normalized to unity at their maximum values. (Although the occultation profiles indicate a smaller relative amplitude for the stratospheric propagation of the smaller harmonic, these are probably constrained there by wave-breaking effects, to be considered in Section 5, and may therefore differ from the true relative amplitudes at depth.) The latitudes of maximum amplitude scale roughly as the fourth root of the equivalent depth (for the same zonal wavenumber and meridional structure index).

An especially interesting property of the Yanai wave is the antisymmetry of its pressure, temperature, and vertical velocity fields, as in the example shown in Fig. 6. Hunt *et al.* (1981) have suggested that the latitudinal asymmetry of the plumes may be attributed to the disruption of their diabatic driving to the south of the equator by the Great Red Spot. Whatever its source, however, the linear response to an asymmetric forcing can be analyzed as a superposition of a symmetric and an antisymmetric mode with the same phase velocity and wavenumber. As a speculative example, chosen to minimize the discrepancy with the diagnostically inferred equivalent depths, the $h = 3$ km Rossby mode and $h = 0.038$ km Yanai mode have the same phase velocity for zonal wavenumber 12. The equatorial asymmetry of the south equatorial chevrons might represent the superposition of an even and odd j index gravity mode with the same equivalent depth and zonal wavenumber ($n \sim 100$), with nearly identical short-wave phase speeds. Although Fig. 6 shows that the conjectured antisymmetrization of modes is imperfectly matched in latitude, this may be modulated by the neglected effects of latitudinal shear.

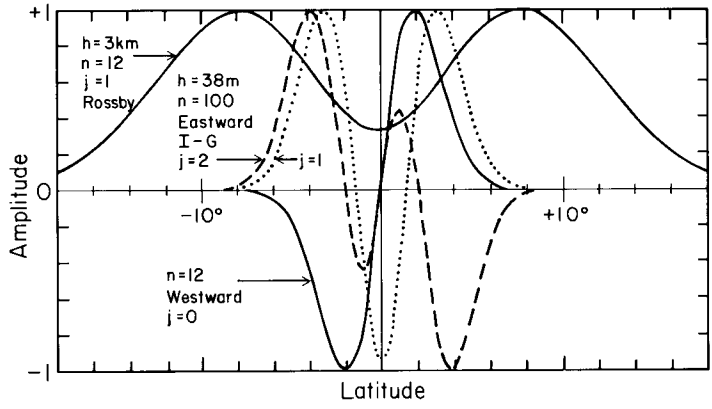

FIG. 6. The meridional structure of the geopotential height field associated with the $h = 3$ km, $n = 12, j = 1$ Rossby mode, the $h = 0.038$ km, $n = 12, j = 0$ westward Yanai mode, and the $h = 0.038$ km, $n = 100, j = 1$ and 2 eastward inertia–gravity modes. The relative amplitudes of the eigenfunctions are normalized to unity at their maximum values.

Despite the uncertainties, the spatial structure and phase speed of the $h \approx 2$–4 km Rossby mode uniquely satisfies the inferred observational constraints on the wave-dynamical interpretation of the plumes. In particular, the associated meridional structure, as exhibited in Figs. 4 and 6, in comparison with the observed latitudinal offset of these features, strongly corroborates their identification as $j = 1$ Rossby modes with a vertical structure comparable to the large harmonic of the radio occultation profiles. The smaller vertical structure harmonic in the occultation profiles may be interpreted as an equatorial gravity mode. Although the gravity modes may be plausibly associated with small scale cloud structures, this identification is somewhat speculative.

4. A VERTICAL STRUCTURE MODEL

The possible maintenance of the diagnostically inferred wave modes may be investigated with a simple four-layer model for the vertical structure. A schematic representation is presented in Fig. 7. Each layer is assumed to have a constant static stability. The uppermost layer (A) represents the region above the 140-mbar tropopause ($\hat{z} \equiv 0$) level, where $\Gamma_A/g = 10$ km as observed. The layer (B) immediately below is assumed to be very weakly stratified, so that $\Gamma_B/g \ll h/4$ and may be approximated as $\Gamma_B/g \approx 0$. At a depth d (scale-heights) below the tropopause there is assumed to be a thin layer (C), of thickness δ, with a stability large enough to support vertical oscillations so that $\Gamma_C/g > h/4$. Such a layer might be supported by the condensation of a massive water cloud, assuming the effect of the Jovian moist convection on the large-scale environment is similar to the terrestrial cumulus dynamics. (A parametric estimate of the possible stability, based on simple considerations of the moist thermodynamics, will be described below.) At levels below the assumed stable layer there is a deep adiabatic layer (D), for which $\Gamma_D = 0$, plausibly maintained by the planet's internal convection. This model has been chosen as the simplest possible representation of a vertical structure, consistent with the stratospheric observations, including a deep stable region, which can act as a (leaky) duct of almost free oscillations. A somewhat different wave duct model has been proposed by Flasar and Gierasch (1986) for the trapping of very small-scale ($n \sim 1000$) gravity waves near Jupiter's ammonia deck by vertical wind shear. In their paper the term

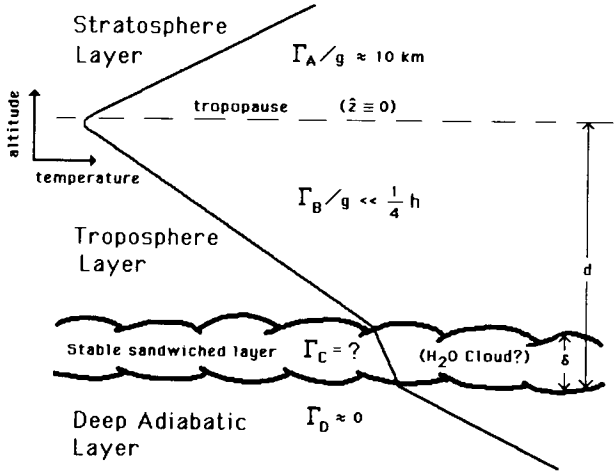

FIG. 7. Schematic illustration of the four-layer vertical structure model for the computation of trapped-free equivalent depths. (See text for details.)

"trapping region" refers to the evanescent layer above the stable duct, while this study adopts the somewhat different terminology of the "stable trapping layer" in reference to the duct itself. Although it is not clear whether their assumed model is compatible with the one adopted here, the two may pertain only to entirely different space and time scales for the motion.

Solutions to the vertical eigenvalue equation (11) for the assumed vertical structure model may be written as

$$\chi = \begin{cases} A_{W/E} e^{\pm i\mu_A \hat{z}} \\ \qquad \text{for} \qquad \hat{z} > 0 & (20a) \\ B_1 e^{+\hat{z}/2} + B_2 e^{-\hat{z}/2} \\ \qquad \text{for } \delta - d < \hat{z} < 0 & (20b) \\ C_1 e^{+i\mu_C(\hat{z}+d-\delta)} + C_2 e^{-i\mu_C(\hat{z}+d-\delta)} \\ \qquad \text{for} \quad -d < \hat{z} < \delta - d & (20c) \\ D e^{+(\hat{z}+d)/2} \\ \qquad \text{for} \qquad \hat{z} < -d. & (20d) \end{cases}$$

The solution for layer A is written so as to satisfy the "radiation condition" of outgoing energy flux as $\hat{z} \to \infty$. This requires the choice of the positive (or negative) sign in the exponential for westward (or eastward) waves with amplitude coefficient A_W (or A_E). (For a further discussion, see Chapter 2 of Holton 1975.) The solution for layer D is written so as to satisfy the "evanescent condition" of vanishing amplitudes for $\hat{z} \to -\infty$. In addition, it is necessary to impose as boundary conditions at each of the layer interfaces the continuity of χ and its first derivative. (These are equivalent to requiring the continuity of normal velocity and geopotential.) Then after some algebra the resulting compatibility condition for the vertical eigenvalue problem becomes

$$\frac{\mu_C}{\mu_C^2 - \frac{1}{4}} = \left[1 + e^{-(d-\delta)} \cdot \frac{(\pm i\mu_A + \frac{1}{2})(\frac{1}{4} + \mu_C^2)}{(\pm i\mu_A - \frac{1}{2})(\frac{1}{4} - \mu_C^2)}\right] \tan(\mu_C \delta) \quad (21)$$

which, for $d - \delta \gg 1$, $\Gamma_C/g \gg h/2$, accurately reduces to

$$\mu_C = (\mu_C^2 - \tfrac{1}{4}) \tan \mu_C \delta, \quad \text{with } \mu_C \equiv (\Gamma_C/gh - \tfrac{1}{4})^{1/2}. \quad (22)$$

As long as the difference between the depth of the stable layer and its thickness is much larger than a pressure scale height, the eigenvalue problem for the equivalent depth is effectively independent of the stability of the upper (stratospheric) layer. Due to the periodicity of the tangent function, this has an infinite number of eigenmodes. There is a degenerate solution, corresponding to $\mu_C \equiv 0$, but by application of the boundary conditions to the general solution (20) is seen to correspond to vanishing wave amplitudes. Figure 8 displays the first two nontrivial values for the equivalent depth, denoted h_0 and h_1, for a selected range of (Γ_C/g) and δ as computed by the numerical solution of (22). The asymptotic analysis of the problem reveals that to fair approximation, within the range of interest, these two

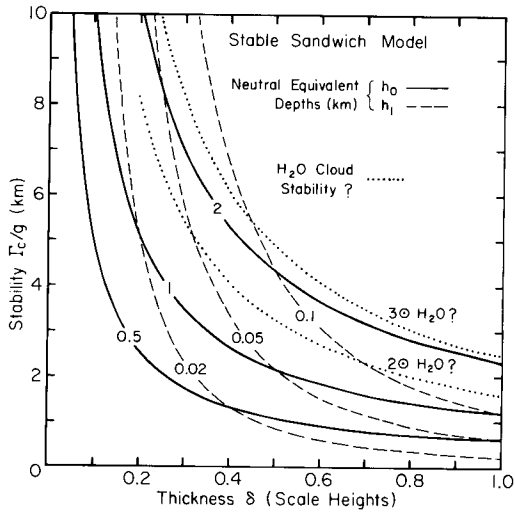

FIG. 8. Neutral equivalent depths corresponding to free solutions of the deep stable trapping model as a function of the stable layer thickness δ (in scale heights) and the static stability Γ_c/g (in km). The solid curves are the equivalent depths for the gravest solution to the vertical structure problem while the dashed curves represent the second (smaller) solutions. The two dotted curves indicate an estimate of the possible static stability for a 2 and 3 solar mixture water cloud, as a function of the thickness of the negatively buoyant depth.

modes are also given by the simple algebraic expressions

$$h_0 \approx \delta(\Gamma_C/g) \tag{23a}$$

and

$$h_1 \approx (\delta/\pi)^2(\Gamma_C/g). \tag{23b}$$

It is of interest to consider the possibility that these first two modes might represent the two equivalent depths diagnostically inferred above. With $h_0 = 2$ km and $h_1 = 0.06$ km, (23) implies $\Gamma_C/g \approx 6.8$ km and $\delta \approx 0.3$. The required stability is several times larger than that observed immediately below the tropopause. (Otherwise, vertical trapping could not occur.) Its magnitude is, however, within reasonable bounds of a simple parametric estimate of the total buoyancy contrast which might be imposed by the condensation of a roughly solar abundant water cloud.

Although the moist convection of individual parcels is effected within columns of unstably stratified fluid, the terrestrial experience suggests that the large-scale environment will be stabilized by the resulting redistribution of heat. As previously suggested by Ingersoll (1976), a similar stabilization of the vertical structure may prevail within the Jovian water cloud. Unless the relative humidity of the environment is fully 100%, a "conditionally unstable" parcel must first attain its "lifting condensation level," where it is saturated by its condensed vapor, before it becomes positively buoyant. For vertical excursions over lesser altitudes the parcel is therefore negatively buoyant (or positively stable). Several numerical examples under Jovian conditions for a variety of assumed environmental humidities have been worked out by Stoker (1986), based on a one-dimensional cloud parcel model. The theory of moist convective disturbances (e.g., Lilly 1960) suggests, however, that conditional instability favors the smallest horizontal scales of motion. This expectation is corroborated by observations of cumulus dynamics in the terrestrial tropics, where the area of active convection is relatively small in comparison to the total, itself largely dominated by dry subsidence. Lunine and Hunten (1987) have proposed a similar configuration for Jupiter. In this case the redistribution of latent heat by narrow moist-convective updrafts and the surrounding dry subsidence will warm the top of the cloud layer, while cooling levels below. The net result, on the large scales of motion exhibited by planetary wave dynamics, is an environmental lapse rate typically intermediate between the moist and the dry adiabats (cf. Ludlam 1980.) Vivid examples of observed moist-convective systems in the terrestrial tropics are reported, for example, by Ogura and Cho (1973) and Lord and Arakawa (1980). Owing to the enormous separation of scales, prognostic weather models are unable to explicitly calculate the full space-time structure of cumulus convection as it is coupled to the large-scale dynamics. The parameterization of the ensemble cloud structure requires some closure assumption as to the actual cloud mass flux, guided by the observations, and is complicated by uncertainties in the entrainment, rainout, and reevaporation rates. A general discussion of this problem, as well as the moist-convective parcel dynamics, is given in the textbook by Haltiner and Williams (1980). Del Genio and McGrattan (1988) have applied a state-of-the-art cumulus convection scheme, tested against terrestrial observations, to Jovian conditions. Their results suggest that the moist-convective transport required to support the planet's internal heat flux will indeed stabilize a layer near the water condensation level, by an amount depending somewhat upon the assumed initialization and the rate of reevaporation of falling condensate.

Gierasch and Conrath (1985) provide a simple parametric estimate for the moist stabilization of the vertical structure based upon a consideration of the combined effects of the differentiation of mean molecular weight $(\Delta m/m) \approx f_{H_2O} \cdot (m_v/m)$ and the

change in temperature due to latent heating $(\Delta T/T) \approx f_{H_2O} \cdot L_v/c_pT_c$. (Here $m \approx 2.2$ denotes the mean molecular weight, $m_v = 18$ the molecular weight of water, f_{H_2O} the water molar fraction, $L_v \approx 2.1 \times 10^7$ J kg^{-1} its molar latent heat of vaporization, and $T_c \approx 290$°K the condensation temperature.) For the case of a Jovian hydrogen–helium mixture enriched in oxygen by a factor $(f_{H_2O}/f_\odot)$ over the solar abundance value $(f_\odot \approx 1.5 \times 10^{-3})$, the recipe of Gierasch and Conrath yields a total buoyancy contrast

$$b = (\Delta m/m) + (\Delta T/T) \approx 0.019 \cdot (f_{H_2O}/f_\odot). \quad (24)$$

If distributed over a thickness δ, this corresponds to an effective static stability

$$\Gamma_C/g = bH/\delta \approx (f_{H_2O}/f_\odot)(0.8 \text{ km})/\delta \quad (25)$$

(where H is the pressure scale-height, taken as 44 km near the water cloud). It should be emphasized that this recipe can only be regarded as a plausible order-of-magnitude estimate of the possible effects of a complicated process, the details of which are still largely unknown.

Figure 8 displays as dotted curves the estimated water cloud stability Γ_C/g as a function of δ according to (25) for molar enrichments of 2 and 3 times the solar composition value. The two curves are seen to bracket the $h = 2$ km eigenvalue for all $\delta \leq 1$. With a water condensation pressure greater than 6 bars, $d \geq 4$ so that solutions to (22) will be valid approximations to the vertical eigenvalue problem for all $\delta \leq 1$. If the effective large-scale stabilization is supported over the full height of towering cumulus convection, δ might be of order unity. Alternatively, if supported by a shallow stratiform configuration, $\delta \cdot H$ could be as small as the saturation scale height, as estimated from the Clausius–Clapeyron equation, with $\delta \geq c_pT_c(m/m_v)/L \approx 0.2$ roughly independent of the molar enrichment factor (cf. Barcilon and Gierasch 1970). The numerical model results of Del Genio and McGrattan (1988) imply moist stabilization over a depth of a scale height or less above the condensation level, but with an associated buoyancy contrast somewhat less than the assumed limiting value of Gierasch and Conrath given above, depending upon the details of the convection. A supersolar abundance of water may therefore be required in order to account for the assumed stable trapping layer.

The actual Jovian water abundance is unfortunately a poorly constrained feature of the model. Recent work by Bjoraker *et al.* (1986) suggests a substantially subsolar water abundance at infrared (5 μm) sounding levels above 7 bars, but with large inferred vertical variations, increasing with depth by a factor of 10 from 4 to 6 bars. If these levels were really below the cloud base associated with a globally depleted water abundance, a uniform mixing of vapor would be expected to prevail there. The radiative transfer analysis of the Voyager IRIS data by Carlson *et al.* (1988) indicates, however, that the water abundance below the cloud base is at least as great as the solar composition value. Studies of Jupiter's equilibrium chemistry conclude that global depletions of water are incompatible with the observed abundances of nitrogen and carbon which are best fitted by a solar enrichment factor of about 2 (cf. Carlson *et al.* 1987, Fegley and Prinn 1988). Models of the Jovian interior by Hubbard and Marley (1989), optimized to match the planet's gravitational harmonics, also imply a solar water abundance for its hydrogen envelope. The real situation may include a latitudinal differentiation of the water in response to the large-scale dynamics (cf. Barcilon and Gierasch 1970), perhaps with an equatorial enrichment of the actual global abundance. *In situ* measurements of the deep thermal structure, cloud properties, and water abundance of Jupiter's north equatorial zone will be provided by the Galileo entry probe.

One other feature of the vertical structure model is worth mentioning here. If the large-scale wave fields, including the verti-

cal velocity, are to be vertically coherent over the full depth of the troposphere (that is, if they are not to change sign for all $\hat{z} < 0$ at a given instant of time), then the thickness of the stable trapping layer must be less than one-half a vertical wavelength there, given as $\pi/\mu_C = \pi/(\Gamma_C/gh - \frac{1}{4})^{1/2}$. (Although there is no observational constraint on this condition, the requirement will be relevant to the consideration of diabatic forcing as discussed in the next session.) By application of the approximate analytic solutions (23a,b), it is evident that the requirement is strongly satisfied for the h_0 mode for all $\delta \leq 1$, but only marginally met for the h_1 mode, for which $\mu_C \approx \pi/\delta$.

To summarize the model results, the larger equivalent depth of $h \approx 2$ km, diagnostically inferred from correlative Voyager observations and interpreted as a zonal wavenumber 12 Rossby wave, is plausibly supported as a nearly trapped free, vertically coherent oscillation within a deep stable water cloud with a roughly three times solar (or perhaps larger) mixing ratio of oxygen. If the thickness of the stable region is only slightly greater than the condensation scale height, the same layer will also trap a second equivalent depth comparable to $h_1 \approx 0.06$ km as inferred for the smaller harmonic structure in the occultation retrievals.

5. FORCING AND DISSIPATION

Although the results of the previous section suggest that equatorial planetary waves associated with the plumes might be supported by the vertical structure as nearly free modes, some forcing mechanism is still required to replenish their "leaky" propagation up through the stratosphere above. Possible sources for planetary wave forcing include diabatic heating and horizontal exchanges of momentum. Although these processes are poorly constrained by the available observations it is nevertheless instructive to consider their effects as weak corrections to the diagnostically inferred eigenmodes.

Hunt *et al.* (1981) have suggested that the equatorial plumes may be generated by latent heat release associated with wave-induced variations in the deep moisture field, as in the so-called "wave-CISK" process in the terrestrial tropics (cf. Lindzen 1974a, Hayashi 1970). "CISK" is an acronym for "conditional instability of the second kind" and refers to the state of an unsaturated but conditionally unstable region of atmosphere for which large-scale, low-level convergence and accompanying rising motion can bring vapor-laden parcels from below to a level where they are at last convective, thereby establishing a feedback among horizontal dynamics, clouds, and heating. On Earth the requisite convergence may be supported either by swirling friction layers (as in hurricanes) or by wave compression (as accompanying periodic cloud clusters within the Inter-Tropical Convergence Zone). An explicit model of the forcing requires the external specification of the diabatic heating Q in the thermodynamic heat equation (6). In terrestrial studies Q is often parameterized in proportion to the vertical velocity at the top of the subcloud convergence zone and with a vertical variation given as some form factor based on observed heating rates. Thus specified, the vertical eigenvalue problem yields a complex-valued equivalent depth which, in combination with the horizontal dispersion relations, implies an imaginary part to the wave frequency, corresponding to exponential growth in time. According to Emanuel (1987), the actual moist convection in the terrestrial tropics acts primarily to redistribute heat already present at the oceanic surface over the full depth of the troposphere, but in a way that nevertheless results in the growth of low-frequency oscillations.

In view of all the uncertainties about the Jovian water cloud and the dynamical effects of a nonrigid lower boundary there, it may be premature to apply an explicit cumulus heating (or convective redistribution) model to the analysis of Jupiter's

equatorial plumes. It is possible that the diabatic forcing is actually supplied by the latent heat release associated with ortho–para hydrogen convection (cf. Conrath and Gierasch 1984). As pointed out by Lindzen (1974a), however, the relative growth rates for diabatic driving may be estimated using the already derived horizontal dispersion relations, provided the forcing occurs "near neutral stability" with an imaginary equivalent depth that is small compared to the real values inferred above. Then with $h = h_r + ih_i$ (using subscripts "r" and "i" to denote real and imaginary parts), $(\sqrt{gh})_i \approx (h_i/2h_r)\sqrt{gh_r}$ and the growth rates are given by the Taylor expansion

$$\sigma_i \approx (h_i/2h_r)(\sqrt{gh_r}) \cdot [d\sigma_r/d\sqrt{gh_r}], \quad (26)$$

where $\sigma_r \approx (n/a)c$. In this near-neutral limit the estimate of the relative growth rates therefore does not depend upon the details of the forcing (nor is necessarily restricted to moist convection).

For Kelvin waves, the imaginary part of the frequency is then given by application of (16) to (26) as

$$\sigma_i(\text{Kelvin}) \approx (h_i/2h_r) \cdot (n/a)\sqrt{gh_r}. \quad (27)$$

For Yanai waves

$$\sigma_i(\text{Yanai}) \approx +\frac{1}{4}\frac{h_i}{h_r}\sqrt{gh_r} \cdot \left\{\frac{n}{a} \pm \frac{1}{2}\frac{[2\sqrt{gh_r}(n^2/a^2) + 4\beta]}{[gh_r(n^2/a^2) + 4\beta\sqrt{gh_r}]^{1/2}}\right\} \quad (28)$$

with the + sign for eastward propagation, and the − sign for westward propagation.

For inertia–gravity waves

$$\sigma_i(\text{I–G}) \approx \pm\frac{1}{4}\frac{h_i}{h_r}\sqrt{gh_r} \cdot \frac{[2(n^2/a^2)\sqrt{gh_r} + \beta(2j+1)]}{[(n^2/a^2)gh_r + \beta(2j+1)\sqrt{gh_r}]^{1/2}}. \quad (29)$$

For Rossby waves

$$\sigma_i(\text{Rossby}) \approx -\frac{1}{2}\frac{h_i}{h_r}\sqrt{gh_r} \cdot \frac{\beta^2(2j+1)(n/a)/gh_r}{[(n^2/a^2) + \beta(2j+1)/\sqrt{gh_r}]^2}. \quad (30)$$

Figure 9 displays the corresponding relative growth rates for $h_r = 2$ km as a function of the zonal planetary wavenumber n. For a fixed choice of h_r and h_i, the growth rates for the Kelvin, eastward Yanai, and inertia–gravity modes increase indefinitely with zonal wavenumber, while the westward Yanai mode maximizes at wavenumber zero. Several studies of terrestrial wave-CISK have devoted considerable effort to understanding how these two limits might be avoided, mostly by allowance for a frequency-dependent or phase-lagged forcing parameter (e.g., Hayashi 1971, Kuo 1975, Davies 1979). The idea is that high frequency oscillations are less efficiently heated by the latent heat release than those with low frequencies, owing perhaps to the finite convective overturning time within the cloud clusters. Without introducing a necessarily somewhat *ad hoc* model for the postulated frequency adjustment, it may at least be verified that except for the low-wavenumber Kelvin modes, which have correspondingly small growth rates, the modes in question have much higher frequencies, by a factor of 10 or so, than the Rossby modes of the same equivalent depth over the entire range of wavenumbers. At any rate, the Rossby modes are the only ones for which the near-neutral estimate of relative growth rates give a nonzero but finite scale selection. For these the growth rates given by (30) maximize at that value of the wavenumber n_m for which

$$n_m = [\beta a^2(2j+1)/3\sqrt{gh}]^{1/2}, \quad (31)$$

so that for $h = 2$ km and $j = 1$, $n_m \approx 11$, in close agreement with the observed number of equatorial plumes.

The evaluation of the absolute growth rates for the Rossby waves requires the specification of h_i as determined from the solution of the vertical structure equation with an explicit forcing model. The diagnostic requirements for the persistent stratospheric propagation of the waves, however, provide an approximate constraint on its size. Away from the forcing

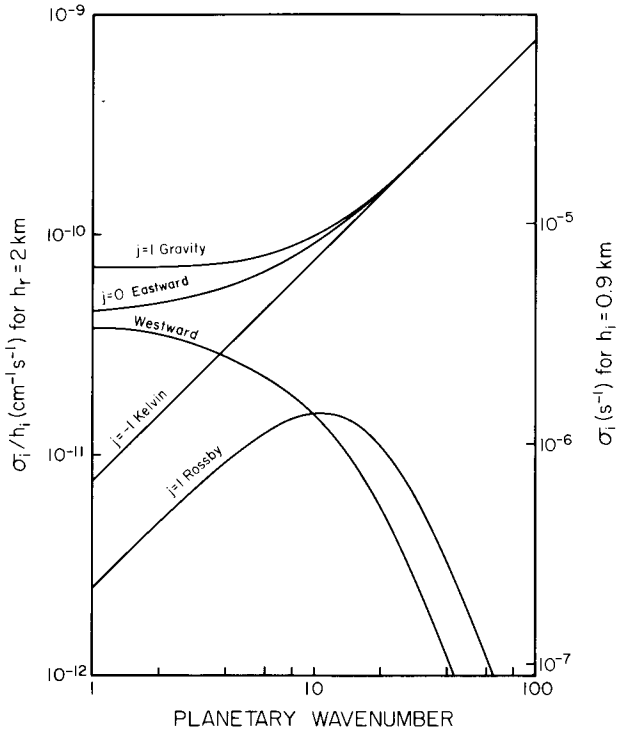

FIG. 9. Relative growth rates as a function of planetary wavenumber for the near-neutral wave-CISK forcing of Jovian equatorial wave modes with a neutral equivalent depth of 2 km. The left-side ordinate is marked for growth rates divided by the imaginary equivalent depth, while the right-side ordinate is calibrated for absolute rates, assuming $|h_i| = 0.9$ km.

region and within a layer of constant static stability, the vertical structure solution and the variable transformation (10) imply that the wave fields propagate as

$$u, v, \hat{w}, \phi, T \propto e^{+\hat{z}/2} e^{i(nx/a \pm \mu\hat{z} - \sigma t)}. \quad (32)$$

For unstably growing waves (with complex equivalent depths) forced near neutral stability, the vertical wavenumber $\mu \approx (\sqrt{\Gamma}/gh_r)[1 - i(h_i/2h_r)]$ (provided $\Gamma/gh_r \gg \frac{1}{4}$). Wave fields associated with upward energy transport will therefore penetrate to all stratospheric elevations provided that

$$|h_i|_{z\to\infty} = (gh_r^3/\Gamma)^{1/2} \approx 0.9 \text{ km} \quad (33)$$

(for $h_r = 2$ km and $\Gamma/g = 10$ km), consistent with the near-neutral assumption that $h_i \ll 2h_r$. If h_i were much larger than this, the wave would decay with height. It could be smaller, with the vertical wave amplitude restricted by dissipation or shear. By assuming this value as an upper limit, however, it is possible to estimate the maximum limiting growth rate for the near-neutral forcing of the $h \approx 2$ km, $n = 11$ Rossby modes. (This methodology is analogous to terrestrial wave-CISK studies in which the vertical variation of the wave and energy amplitudes for the calculated forcing is constrained by direct observations of the tropical atmosphere (cf. Hayashi 1970, Davies 1979).) The right-side ordinate of Fig. 9 is calibrated for this value of h_i and shows a maximum growth rate of about 1.4×10^{-6} sec^{-1} for the Rossby modes, corresponding to a growth time of about 20 Jovian days. For comparison, Hunt *et al.* (1982) report substantial increases in the bright areas of the most active equatorial plume features over periods less than 50 Jovian rotations.

Diabatic heating may not be an efficient driver for the smaller equivalent depth of $h_1 \approx 0.04$–0.06 km, since it only marginally satisfies the vertical wave coherency condition as defined in the previous section. This is supposedly a necessary requirement for the organization of large-scale vertical motions and moist convection, since up and down motions will otherwise compete with each other within a single column of conditionally unstable atmosphere (cf. Lindzen 1974a). The smaller equivalent depth might be driven as the near-resonant response of the Yanai mode with a phase speed and zonal wavenumber comparable to that of the north equatorial plumes. Alternatively, the smaller harmonic may exist as a gravity mode vertically ducted by the local vertical shear at the ammonia deck (cf. Flasar and Gierasch 1986).

The south equatorial plume feature also fails to find a ready identification as a diabatically forced mode but appears to interact strongly with the Great Red Spot (GRS) which, as Hunt *et al.* (1981) suggest, may effectively disrupt any organized moist-convective forcing in this region. It may be conjectured that the southern plume arises as the wavenumber-one response of an $h \approx 2$ km Rossby mode to meridional exchanges of momentum with the adjacent GRS latitude.

In the presence of forcing, either by diabatic or eddy momentum exchanges, some form of dissipation is also required in order to maintain an equilibrated response and may also affect the vertical propagation. Chang and Lim (1982) have shown, for example, that the equivalent depth of the $j = 1$ Rossby mode for a given phase speed is increased by the inclusion of damping as estimated for the terrestrial tropics. The strength of the momentum dissipation in Jupiter's deep atmosphere is unknown. Moist convection in the deep troposphere may impose a vertical exchange of momentum as in the cumulus "friction" models for tropical wave motion on the Earth (cf. Stevens *et al.* 1977) but cannot be assessed from remote sensing data. In the stratosphere, however, the breaking of vertically propagating, large-amplitude waves may itself act as a dissipative process and is tentatively indicated by the radio occulation profiles.

Wave breaking is expected to occur wherever the local lapse rate imposed by a wave exceeds the adiabatic value (cf. Lindzen 1981). For a two-component stratospheric propagation superimposed upon the ambient static temperature there, the local wave-induced thermal profile may be expressed as

$$T = T^{a}(\hat{z}) + \Delta T_1 e^{i\mu_1 \hat{z}} + \Delta T_2 e^{i\mu_2 \hat{z}}, \quad (34)$$

where ΔT_1 and ΔT_2 are the amplitudes of the two components and $\mu_1 \approx 2.1$ and $\mu_2 \approx 13$ are their stratospheric wavenumbers as indicated by the radio occultation profiles. The minimum difference between the lapse rate associated with the two-component propagation and the adiabatic value is

$$|dT/d\hat{z} + RT/c_p|_{\min} \approx \Gamma/R - \mu_1 \Delta T_1 - \mu_2 \Delta T_2 \quad (35)$$

(assuming $\Delta T_1, \Delta T_2 \ll T^{a}$) which is negative for

$$\Delta T_2 > \mu_2^{-1}[\Gamma/R - \mu_1 \Delta T_1]. \quad (36)$$

Then with $\Delta T_1 \approx 10$°K as indicated by the model fit to the radio occultation profile (cf. Fig. 3), wave breaking will occur for $\Delta T_2 > 3$°K, comparable to the amplitude of the smaller harmonic. Although this may be a slight overestimate of the minimum amplitude in the presence of wind shear, it nevertheless indicates the plausible occurrence of wave breaking in the Jovian equatorial stratosphere.

Assuming that wave breaking is occurring, it is of interest to estimate the strength of the associated turbulent dissipation. There is an established procedure for this based upon the assumption that wave breaking generates an effective eddy dissipation analogous to molecular diffusion which acts to cancel the exponential growth of the amplitudes with altitude (cf. Hodges

1969, Hines 1970, French and Gierasch 1974, Lindzen 1981). According to this model, the dissipation terms in (2), (3), and (6) may be parameterized as

$$\mathfrak{D}\mathbf{x}, \mathfrak{D}\mathbf{y}, \mathbf{Q} \approx \frac{\nu_{\text{eddy}}}{H^2} \frac{\partial^2}{\partial \hat{z}^2} (u, v, T), \quad (37)$$

where ν_{eddy} denotes the coefficient of eddy viscosity (in cm^2/sec) and H is the scale height. The inclusion of these terms in the momentum and heat equations is equivalent to including an imaginary contribution to the phase speed so that

$$c \approx c_r + i(a/nH^2)\mu^2 \nu_{\text{eddy}}, \quad (38)$$

where c_r denotes the real part (as estimated for an undamped wave). Substitution into the dispersion relations gives, after straightforward manipulation (exploiting the assumed relative smallness of the imaginary contribution),

$$\mu_i \approx -(a/ncH^2)\mu^3 \nu_{\text{eddy}}. \quad (39)$$

The same expression may be obtained for long-wave Rossby modes (although c and μ are different in that case). Then the eddy viscosity generated by stratospheric wave breaking may be crudely estimated by specifying the size of this so as to just cancel the effect of the exponential variation of the wave solutions with altitude as in Eq. (32) above. When, according to arguments presented by Lindzen (1981), allowance is also made for the additional vertical variation of the amplitudes as a result of vertical wind shear, this becomes

$$\nu_{\text{eddy}} \sim |ncH^2/2a\mu^3|[1 + (3/c)(dU/d\hat{z})]. \quad (40)$$

The numerical factor for the wind shear term arises from the analysis of the WKB solution for the vertical structure, accounting for a slow variation of the vertical wavenumber in response to the Doppler shifted phase speed. (Although Lindzen's treatment is specifically developed for internal gravity modes, a similar analysis may be performed for the long-wave equatorial Rossby modes with the same result, when expressed in the form given here.) According to this recipe, the requisite size of the eddy viscosity for the vertical attenuation of the amplitudes of eastward propagating modes is somewhat reduced by the presence of negative vertical shear. If $-dU/d\hat{z}$ becomes as large as $c/3$, the amplitudes of eastward gravity modes would be constrained without any eddy mixing. For the westward propagating Rossby modes, however, negative vertical shear only exacerbates the dissipation required according to this estimate.

For an $n = 100$, $h \approx 0.06$ km ($\mu \approx 13$) eastward inertia–gravity mode, Eq. (40) yields, in the absence of shear, a maximum value of $\nu_{\text{eddy}} \sim 7 \times 10^4$ cm^2 sec^{-1}. If the Rossby mode is also breaking, then with $n = 12$, $h \approx 2$ km, and $\mu \approx 2$, Eq. (40) implies a somewhat larger value of ν_{eddy} $\sim 2 \times 10^6$ cm^2 sec^{-1}, although this would only be applicable to motions with a vertical extent greater than a scale height. It is comparable, however, to the equatorial eddy diffusion coefficient at the homopause (near the microbar pressure level) estimated by Atreya *et al.* (1981), based on the analysis of Voyager UVS stellar occultation data. In the absence of strong vertical shear, the equatorial Rossby waves may therefore propagate to very high levels before they are attenuated. Stratospheric wave breaking may contribute to the deceleration of the mean zonal flow, as modeled by Gierasch *et al.* (1986). Although Lindzen (1981) has emphasized that the wave deceleration process is not adequately represented as linear Rayleigh friction, the diagnostic identification of propagating wave modes in this study may provide a useful starting point for further work on this problem.

If the stratospheric wind decreases strongly with altitude, the Rossby waves will be absorbed at their so-called critical level, where the vertically integrated shear exceeds the reference phase velocity below. Above such a level the westward phase drift can no longer prevail as a verti-

cally coherent structure and the wave will be torn apart. The persistence of harmonic oscillation over some four scale heights in the radio occultation profiles suggests, however, that this does not occur in the lowest part of the stratosphere. Short of a critical level, the Rossby frequency and phase speed will undergo a vertically varying Doppler shift, with the equivalent depth no longer constant but decreasing with elevation in order to satisfy the horizontal dispersion relation. The analysis of the vertical variation of amplitudes and energy in this case is necessarily elaborate (cf. Lindzen 1972) and surpasses the present observational definition of the problem. The validity of the simple four-layer vertical structure model also demands that the difference in the wind velocity between the cloud-tracked level and the assumed stable trapping layer be less than about 50 m sec^{-1}. Otherwise, critical level absorption would probably prevent any waves vertically ducted at deep levels from propagating into the stratosphere. While the possibility of a very weakly sheared zonal flow, extending to a depth of several scale heights below the cloud tops, has been advocated by several authors (e.g., Ingersoll and Pollard 1982, Kirk and Stevenson 1987), the requirements might also be satisfied for a shallow layer by the deferment of strong vertical shears to levels just below the water cloud.

6. SUMMARY AND DISCUSSION

The primary objective of this study has been the identification of a distinguishing class of planetary wave modes in interpretation of Voyager imaging, infrared, and radio science observations of large-scale periodic structure in Jupiter's equatorial atmosphere, with special attention to the equatorial plume features. The comparative assessment of the horizontal dispersion properties for linear wave modes on an equatorial beta plane suggests that the Rossby modes with a meridional structure index $j = 1$ and an equivalent depth of $h \approx$ 2–4 km are the most plausible interpretation, consistent with all the observations, for an equatorially trapped, wavenumber 12 pattern as well as the single ($n = 1$) plume feature to the south of the equator. The inertia–gravity modes are also suggested in interpretation of smaller scale periodic structure in both the imaging and the radio occultation data. Although it cannot be definitely identified, the Yanai mode (with an equivalent depth $h \approx 0.04$ km) may arise as a response to the asymmetric forcing of the equatorial region. A summary of these tentatively identified planetary wave modes is given in Table I. In view of the necessarily imprecise determination of the equivalent depth, as well as its possible variation with dissipation and vertical shear, this parameter is given in terms of a range of estimates suggested by the considerations discussed above. The vertical wavelength and horizontal phase speeds vary roughly as the square root of this parameter, while the meridional structure depends only on its fourth root.

A secondary objective of this study has been the identification of plausible mechanisms for the stable maintenance, forcing, and attenuation of the inferred wave modes, with attention to what may be learned about the associated structure of both the deep troposphere and upper stratosphere. A simple vertical structure model with a deep stable trapping layer, sandwiched above and below by a nearly adiabatic troposphere, appears to be consistent with the inferred equivalent depths, provided its effective static stability is as large as might be imposed by a supersolar abundant water cloud. Although the detailed effects of this are uncertain, the simple moist stabilization recipe of Gierasch and Conrath (1985) demands a water enrichment of roughly two to three times the solar abundance value in order to trap the inferred wave modes in the assumed way.

It is possible that the stability for a shallow sandwiched layer could be provided by the disequilibration of ortho–para hydrogen

TABLE I

SUMMARY OF TENTATIVELY IDENTIFIED PLANETARY WAVE MODES IN JUPITER'S EQUATORIAL ATMOSPHERE

Wave mode	Planetary wavenumber, n	Equiv. depth, h (km)	Relevant features/ observation	Possible source/driver
		(Large-scale plumes and associated thermal structure)		
Rossby ($j = 1$)	11–13	1–5	N. equatorial plumes, IRIS, Radio Science data (large harmonic).	Vertically ducted and forced (by H_2O cloud?)
Rossby ($j = 1$)	1	1–5	S. equatorial plume	Vertically ducted (and driven by GRS?)
		(Other features—speculatively interpreted)		
Inertia–gravity? ($j = 1, 2$?)	50–100?	~0.06?	Radio science data (small harmonic), S. eqtr. "chevrons"?	Vertically ducted (by clouds and/or wind shear)
Yanai ($j = 0$)??	11–13	~0.06?	Equatorial asymmetry (?)	Antisymmetric response to Rossby mode?

(cf. Conrath and Gierasch 1984) at tropospheric levels above the water cloud, but it is difficult to assess this idea without better measurements or models of the coupling of this process to large-scale motions. Alternatively, the diagnostically inferred equivalent depth may be forced rather than vertically trapped as an almost free mode. In the terrestrial tropics, for example, cumulus heating may force an equivalent depth, on the order of 10 m (cf. Lindzen 1974a,b), much smaller than the free-oscillation value of ~10 km (cf. Holton 1975). It is difficult, however, to imagine a more plausible candidate for the thermodynamic forcing of the vertical structure on Jupiter than either water condensation or the disequilibration of hydrogen. In a relevant sense, the adopted recipe of Gierasch and Conrath (1985) for the effective static stability of an atmospheric condensate may be regarded as a parameterization of an essentially diabatic process.

Although highly idealized, the simple vertical structure model does corroborate the plausibility of the $h \approx 2$ km equivalent depth inferred directly from the large vertical stratospheric wavelength of the radio occultation profiles and indirectly from the consideration of the horizontal dispersion and meridional structure properties of equatorially trapped planetary waves. It is of interest that the implied vertical structure parameter is nearly the same as that adopted for different reasons by Williams and Yamagata (1984) and Williams and Wilson (1988) for their numerical simulation of Jovian atmospheric dynamics with a "shallow water" model. These studies assume the midlatitude deformation radius to be $L_R = (\sqrt{gh})/\Omega \approx 1000$ km, largely based on plausible constraints on the drift speed of solitary vortices, and corresponds to an equivalent depth $h \approx 1$ km.

The assumption of linear wave solutions and the neglect of latitudinal shear are also obvious limitations for this study but have of necessity been adopted to maintain a tractable diagnostic analysis. The nonlinear study of isolated Rossby voritices by Williams and Wilson (1988) again offers several interesting comparisons. Their numerical experiments suggest that stable anticyclones can exist at the equator only with "Korteweg–DeVries longitudinal form" (as nonlinear solitons) but with a latitudinal structure of the same Hermite polynomial form as the linear wave modes of this study. The westward drift realized by the simulated equatorial vortices is generally

larger than the linear long-wave limit but only by about 20%. Williams and Wilson also calculate the effect on their solutions of strong latitudinal shear. Their results indicate a latitudinal expulsion of the higher order ($j = 3$ and 5) Rossby modes in proportion to the size of the zonal wavenumber, while the low wavenumber $j = 1$ mode remains in place, with some meridional elongation beyond the latitude of its maximum amplitude. Although the shear of the equatorial jet assumed by Williams and Wilson is somewhat larger than observationally indicated for Jupiter, the results lend credence to the diagnosis of $j = 1$ Rossby modes within a horizontally uniform flow. The inferred sensitivity of high-wavenumber modes to expulsion by shear suggests, however, that the shape of the inertia–gravity modes shown in Fig. 6 may actually be stretched beyond the indicated latitude. Williams and Wilson are unfortunately unable to simulate a stable, long-lived pattern of wavenumber 12 Rossby vortices. It would be of interest to see how these experiments might vary with a latitudinal wind profile with positive zonal curvature near the equator as observed, or with the inclusion of some diabatic forcing to offset the tendency of vortices to collapse and coalesce.

The motion of the plumes, with respect to the ambient, vertically sheared flow, should be amenable to observational test by the Galileo atmospheric entry probe, now targeted for the north equatorial plume latitudes. The comparison of the results of the Doppler-tracked wind experiment with cloud-tracked wind determinations by the orbiter, together with a calibration of visible cloud levels by the atmospheric structure instrument, neutral mass spectrometer, and nephelometer on the probe, should unambiguously distinguish the reality of a relative phase drift as large as 50 m sec^{-1}. According to studies by Atkinson (1989) the accuracy of the probe Doppler wind experiment will be sufficient to distinguish differences as small as a few meters per second. The various probe instruments will also provide a test of the vertical structure model, including its assumption of a massive water cloud. Further radio occultation measurements of stratospheric temperature profiles at the equator, if they can be obtained, will also contribute importantly to the further diagnosis of planetary waves. If the wave dynamical interpretation is correct, then these observations may provide an important window to atmospheric structure at levels where it may be difficult to obtain accurate soundings directly, even with the entry probe. The sensitivity of vertical wave structure to the static stability at deep tropospheric levels, for example, may exceed the accuracy of the atmospheric structure experiment. At stratospheric levels, in contrast, the accurate inference of the vertical shear of the zonal mean wind from probe Doppler tracking may require a careful analysis of the amplitudes of the horizontal wave motions as constrained by better determinations of the vertical temperature variations.

APPENDIX: THE COMPLETE $y - \hat{z}$ STRUCTURE FIELDS

In the absence of forcing, dissipation, and shear, the full solutions for the eastward and vertical wave velocities as well as the geopotential and temperature fields may be obtained by substituting into the equations of motion and heat (2)–(6) the solution for the meridional variable $v(y, \hat{z})$, given by Eq. (8) in terms of the vertical and horizontal structure variables χ and ψ. χ is the solution to the vertical structure equation (11) while ψ is given in terms of the Hermite polynomials as specified by (12). As a source of reference to the interested reader, the explicit expressions for the complete $y - \hat{z}$ structure of all five wave fields (in terms of χ and ψ) are given here:

$$u = [e^{+\hat{z}/2}(d/d\hat{z} - \tfrac{1}{2})\chi] \cdot [-ih(a/n)(1 - c^2/gh)^{-1}] \cdot (d/dy - \beta yc/gh)\psi \quad \text{(A1)}$$

$$v = [e^{+\hat{z}/2}(d/d\hat{z} - \tfrac{1}{2})\chi] \cdot (-h)\psi \quad \text{(A2)}$$

$$\hat{w} = [e^{+\hat{z}/2}\chi] \cdot [(-c^2/g)(1 - c^2/gh)^{-1}] \cdot (d/dy - \beta y/c)\psi \quad \text{(A3)}$$

$$\phi = [e^{+\hat{z}/2}(d/d\hat{z} - \tfrac{1}{2})\chi] \cdot [-ih(ac/n)(1 - c^2/gh)^{-1}] \cdot (d/dy - \beta y/c)\psi \quad \text{(A4)}$$

$$T = [e^{+\hat{z}/2}\chi] \cdot [i(ac/n)(\Gamma/gR)(1 - c^2/gh)^{-1}] \cdot (d/dy - \beta y/c)\psi. \quad \text{(A5)}$$

The full $(x, y, \hat{z}, t)$ solutions are then given as the real parts of the product of each of these with $e^{i(n/a)(x-ct)}$, where c is given as the wave phase speed with respect to the mean flow by the appropriate choice of Eqs. (16)–(19). The comparative inspection of the above expressions clearly reveals the advantage of initially solving for the meridional velocity in preference to any of the other wave fields. Selected examples of the shape of the meridional form factors for $\hat{w}$, ϕ, and T are displayed in Fig. 6.

ACKNOWLEDGMENTS

I am especially grateful to Joseph Chamberlain for encouraging me with the initial stage of this work which I began while a graduate student at Rice University and to Peter Gierasch for first introducing me several years ago to the theory of planetary wave dynamics during my visit to Cornell. A portion of the study reported here was prepared for presentation at the 1987 Flagstaff Workshop on Time-Variable Phenomena in the Jovian System, and I thank Michael J. S. Belton and Robert West for organizing that meeting and encouraging me to bring this work to publication. I thank my colleagues Barbara Carlson, Anthony Del Genio, and Larry Travis for helpful discussions of this work. Julio Magalhaes and an anonymous referee contributed several valuable suggestions for improving the presentation. The figures were drafted by Christine Dunning, Lilly del Valle, and Jose Mendoza. This research was supported during its final stage of preparation by the NASA Planetary Atmospheres Program managed by Henry Brinton and Jay Bergstralh.

REFERENCES

APPLEBY, J. F., AND J. S. HOGAN 1984. Radiative–convective equilibrium models of Jupiter and Saturn. *Icarus* **59,** 336–366.

ATKINSON, D. H. 1989. *Measurement of Planetary Wind Fields by Doppler Monitoring of an Atmospheric Entry Vehicle*. Ph.D. dissertation, Washington State University.

ATREYA, S. K., T. M. DONAHUE, AND M. C. FESTOU 1981. Jupiter: Structure and composition of the upper atmosphere. *Astrophys. J.* **247,** L43–L47.

BARCILON, A., AND P. GIERASCH 1970. A moist, Hadley cell model for Jupiter's cloud bands. *J. Atmos. Sci.* **27,** 550–560.

BEER, T. 1978. Tropical waves. *Rev. Geophys. Space Phys.* **16,** 567–582.

BJORAKER, G. L., H. P. LARSON, AND V. G. KUNDE 1986. The abundance and distribution of water vapor in Jupiter's atmosphere. *Astrophys. J.* **311,** 1058–1072.

CARLSON, B. E., A. A. LACIS, AND W. B. ROSSOW 1988. Effect of longitudinal variations in relative humidity on the 5 μm spectrum of Jupiter. *Bull. Amer. Astron. Soc.* **20,** 869.

CARLSON, B. E., M. J. PRATHER, AND W. B. ROSSOW 1988. Cloud chemistry on Jupiter. *Astrophys. J.* **322,** 559–572.

CHANG, C. 1970. Westward propagating cloud patterns in the tropical Pacific as seen from time-composite satellite photographs. *J. Atmos. Sci.* **27,** 133–138.

CHANG, C.-P., AND H. LIM 1982. On the effects of viscous damping on equatorial Rossby waves. *J. Atmos. Sci.* **39,** 1726–1733.

COFFEEN, D. L. 1974. Optical polarization measurements of the Jupiter atmosphere at 103° phase angle. *J. Geophys. Res.* **79,** 3645–3652.

CONRATH, B. J., AND P. J. GIERASCH 1984. Global variation of the para hydrogen fraction in Jupiter's atmosphere and implications for dynamics on the outer planets. *Icarus* **57,** 184–204.

DAVIES, H. C. 1979. Phase-lagged wave-CISK. *Q. J. R. Meteorol. Soc.* **105,** 325–353.

DEL GENIO, A. D., AND K. B. MCGRATTAN 1988. Effects of moist convection on Jovian water depletion and static stability. *Bull. Amer. Astron. Soc.* **20,** 868–869.

EMANUEL, K. A. 1987. An air–sea interaction model of intraseasonal oscillations in the tropics. *J. Atmos. Sci.* **44,** 2324–2340.

FEGLEY, B., JR., AND R. G. PRINN 1988. Chemical constraints on the water and total oxygen abundance in the deep atmosphere of Jupiter. *Astrophys. J.* **324,** 621–625.

FLASAR, F. M., AND P. J. GIERASCH 1986. Mesoscale waves as a probe of Jupiter's deep atmosphere. *J. Atmos. Sci.* **43,** 2683–2707.

FOCAS, J. H., AND C. J. BANOS 1964. Photometric study of the atmospheric activity on the planet Jupiter and peculiar activity in its equatorial area. *Ann. Astrophys.* **27,** 36–45.

FRENCH, R. G., AND P. J. GIERASCH 1974. Waves in the Jovian upper atmosphere. *J. Atmos. Sci.* **31,** 1707–1712.

GIERASCH, P. J., AND B. J. CONRATH 1985. Energy conversion processes in the outer planets. In *Recent*

Advances in Planetary Meteorology (G. Hunt, Ed.), pp. 121–146. Cambridge Univ. Press, Cambridge.

GIERASCH, P. J., B. J. CONRATH, AND J. A. MAGALHAES 1986. Zonal mean properties of Jupiter's upper troposphere from Voyager infrared observations. *Icarus* **67,** 456–483.

HALTINER, G. J., AND R. T. WILLIAMS 1980. *Numerical Prediction and Dynamic Meteorology,* 2nd ed. Wiley, New York.

HAYASHI, Y. 1970. A theory of large-scale equatorial waves generated by condensation heat and accelerating the zonal wind. *J. Meteorol. Soc. Japan* **48,** 140–160.

HAYASHI, Y. 1971. Instability of large-scale equatorial waves with a frequency-dependent CISK parameter. *J. Meteorol. Soc. Japan* **49,** 59–62.

HINES, C. O. 1970. Eddy diffusion coefficients due to instabilities in internal gravity waves. *J. Geophys. Res.* **75,** 3937–3939.

HODGES, R. R. 1969. Eddy diffusion coefficients due to instabilities in internal gravity waves. *J. Geophys. Res.* **74,** 4087–4090.

HOLTON, J. R. 1970. A note on forced equatorial waves. *Mon. Wea. Rev.* **98,** 614–615.

HOLTON, J. R. 1975. *The Dynamic Meteorology of the Stratosphere and Mesosphere.* American Meteorological Society, Boston.

HUBBARD, W. B., AND M. S. MARLEY 1989. Optimized Jupiter, Saturn, and Uranus interior models. *Icarus* **78,** 102–118.

HUNT, G. E., B. J. CONRATH, AND J. A. PIRRAGLIA 1981. Visible and infrared observations of Jovian plumes during the Voyager encounter. *J. Geophys. Res.* **86,** 8777–8781.

HUNT, G. E., J-P. MULLER, AND P. GEE 1982. Convective growth rates of equatorial features in the Jovian atmosphere. *Nature (London)* **295,** 491–494.

INGERSOLL, A. P. 1976. Pionerr 10 and 11 observations and the dynamics of Jupiter's atmosphere. *Icarus* **29,** 245–253.

INGERSOLL, A. P., R. F. BEEBE, S. A. COLLINS, G. E. HUNT, J. L. MITCHELL, P. MULLER, B. A. SMITH, AND R. J. TERRILE 1979. Zonal velocity and texture in the Jovian atmosphere inferred from Voyager images. *Nature (London)* **280,** 773–775.

INGERSOLL, A. P., R. F. BEEBE, J. L. MITCHELL, G. W. GARNEAU, G. M. YAGI, AND J-P. MULLER 1981. Interaction of eddies and mean zonal flow on Jupiter as inferred from Voyager 1 and Voyager 2 images. *J. Geophys. Res.* **86,** 8733–8743.

INGERSOLL, A. P., AND D. POLLARD 1982. Motion in the interiors and atmospheres of Jupiter and Saturn: Scale analysis, anelastic equations, barotropic stability criterion. *Icarus* **52,** 62–80.

KIRK, R. L., AND D. J. STEVENSON 1987. Hydromagnetic constraints on deep zonal flow in the giant planets. *Astrophys. J.* **316,** 836–846.

KUO, H. L. 1975. Instability theory of large-scale disturbances in the tropics. *J. Atmos. Sci.* **32,** 2229–2245.

LILLY, D. K. 1960. On the theory of disturbances in a conditionally unstable atmosphere. *Mon. Wea. Rev.* **88,** 1–17.

LIMAYE, S. S. 1986. Jupiter: New estimates of the mean zonal flow at the cloud level. *Icarus* **65,** 335–352.

LIMAYE, S. S. 1987. Color differences in cloud level circulation on Jupiter. *Bull. Amer. Stron. Soc.* **19,** 836.

LIMAYE, S. S., H. E. REVERCOMB, L. A. SROMOVSKY, R. J. KRAUSS, D. A. SANTEK, AND V. E. SUOMI 1982. Jovian winds from Voyager 2. I. Zonal mean circulation. *J. Atmos. Sci.* **39,** 1413–1432.

LINDAL, G. F., G. E. WOOD, G. S. LEVY, J. D. ANDERSON, D. N. SWEETNAM, H. B. HOTZ, B. J. BUCKLES, D. P. HOLMES, P. E. DOMS, V. R. ESHLEMAN, G. L. TYLER, AND T. A. CROFT 1981. The atmosphere of Jupiter: An analysis of the Voyager radio occultation measurements. *J. Geophys. Res.* **86,** 8721–8727.

LINDZEN, R. S. 1967. Planetary waves on beta-planes. *Mon. Wea. Rev.* **95,** 441–451.

LINDZEN, R. S. 1972. Equatorial planetary waves in shear, II. *J. Atmos. Sci.* **29,** 1452–1463.

LINDZEN, R. S. 1974a. Wave-CISK in the tropics. *J. Atmos. Sci.* **31,** 156–179.

LINDZEN, R. S. 1974b. Wave-CISK and tropical spectra. *J. Atmos. Sci.* **31,** 1447–1449.

LINDZEN, R. S. 1981. Turbulence and stress owing to gravity wave and tidal breakdown. *J. Geophys. Res.* **86,** 9707–9714.

LORD, S. J., AND A. ARAKAWA 1980. Interaction of a cumulus cloud ensemble with the large-scale environment, II. *J. Atmos. Sci.* **37,** 2677–2692.

LUDLAM, F. H. 1980. *Clouds and Storms: The Behavior and Effect of Water in the Atmosphere.* Pennsylvania State Univ. Press, University Park.

LUNINE, J. I., AND D. M. HUNTEN 1987. Moist convection and the abundance of water in the troposphere of Jupiter. *Icarus* **69,** 566–570.

MAGALHAES, J. A., A. L. WEIR, P. J. GIERASCH, AND S. LEROY 1987. Vertical wind shear and longitudinal structure in Jupiter's atmosphere. I. Voyager imaging results. *Bull. Amer. Astron. Soc.* **19,** 836.

MAXWORTHY, T. 1985. Measurements and interpretation of a Jovian, near-equatorial feature. *Planet. Space Sci.* **33,** 987–991.

MITCHELL, J. L., R. J. TERRILE, B. A. SMITH, J-P. MULLER, A. P. INGERSOLL, G. E. HUNT, S. A. COLLINS, AND R. F. BEEBE 1979. Jovian cloud structure and velocity fields. *Nature (London)* **280,** 776–778.

OGURA, Y., AND H-R. CHO 1973. Diagnostic determination of cumulus cloud populations from observed large-scale variables. *J. Atmos. Sci.* **30,** 1276–1286.

PEDLOSKY, J. P. 1987. *Geophysical Fluid Dynamics,* 2nd ed. Springer-Verlag, New York.

PEEK, B. M. 1981. *The Planet Jupiter: The Observer's Handbook* (Revised ed. with P. Moore). Faber & Faber, Boston.

SALPETER, E. E., AND D. J. STEVENSON 1976. Heat transport in a stratified two-phase fluid. *Phys. Fluids* **19,** 502–509.

SMITH, B. A., L. A. SODERBLOM, T. V. JOHNSON, A. P. INGERSOLL, S. A. COLLINS, E. M. SHOEMAKER, G. E. HUNT, H. MASURSKY, M. H. CARR, M. E. DAVIES, A. F. COOK II, J. BOYCE, G. E. DANIELSON, T. OWEN, C. SAGAN, R. F. BEEBE, J. VEVERKA, R. G. STROM, J. F. MCCAULEY, D. MORRISON, G. A. BRIGGS, AND V. E. SUOMI 1979a. The Jupiter system through the eyes of Voyager 1. *Science* **204,** 951–972.

SMITH, B. A., L. A. SODERBLOM, R. BEEBE, J. BOYCE, G. BRIGGS, M. CARR, S. A. COLLINS, A. F. COOK II, G. E. DANIELSON, M. E. DAVIES, G. E. HUNT, A. INGERSOLL, T. V. JOHNSON, H. MASURSKY, J. MCCAULEY, D. MORRISON, T. OWEN, C. SAGAN, E. M. SHOEMAKER, R. STROM, V. E. SUOMI, AND J. VEVERKA 1979b. The Galilean satellites and Jupiter: Voyager 2 imaging science results. *Science* **206,** 927–950.

STEVENS, D. E., R. S. LINDZEN, AND L. J. SHAPIRO 1977. A new model of tropical waves incorporating momentum mixing by cumulus convection. *Dyn. Atmos. Oceans* **1,** 365–425.

STOKER, C. R. 1986. Moist convection: A mechanism for producing the vertical structure of the Jovian equatorial plumes. *Icarus* **67,** 106–125.

WALLACE, J. M., AND C. P. CHANG 1969. Spectral analysis of large scale wave disturbances in the tropical lower troposphere. *J. Atmos. Sci.* **26,** 1010–1025.

WILLIAMS, G. P., AND R. J. WILSON 1988. The stability and genesis of Rossby vortices. *J. Atmos. Sci.* **45,** 207–241.

WILLIAMS, G. P., AND T. YAMAGATA 1984. Geostrophic regimes, intermediate solitary vortices, and Jovian eddies. *J. Atmos. Sci.* **41,** 453–478.